Supplemental Material for "Correlated photon dynamics in dissipative Rydberg media"

Emil Zeuthen,[1,2] Michael J. Gullans,[3] Mohammad F. Maghrebi,[3] and Alexey V. Gorshkov[3]

[1] *Niels Bohr Institute, University of Copenhagen, DK-2100 Copenhagen, Denmark*
[2] *Institute for Theoretical Physics & Institute for Gravitational Physics (Albert Einstein Institute), Leibniz Universität Hannover, Callinstraße 38, 30167 Hannover, Germany*
[3] *Joint Quantum Institute and Joint Center for Quantum Information and Computer Science, National Institute of Standards and Technology and University of Maryland, College Park, Maryland 20742, USA*

I. SUCCESSIVE PROJECTIONS OF THE POLARITON WAVE FUNCTION

In this Appendix, we comment further on the process by which the polariton wave train is generated in the medium. In particular, in Fig. 2(b) of the main text, we assumed that the second scattering event occurs when the polariton has not passed the first blockade radius of the medium. In this Appendix, we comment on what happens if a scattering event occurs when the polariton straddles the rear of the first blockade radius of the medium.

As discussed in the main text, the temporal extent of the polariton wave function is defined near the beginning of the medium [Fig. S1(a,b)]. Within the validity of the hard-sphere model, scattered photons are ignorant as to the precise distance to the scatterer, since the scattering event constitutes a projective, binary distance measurement. As a consequence, when a polariton (whose temporal extent was defined near the entrance) straddles the rear of the first blockade radius of the medium [Fig. S1(c)], then a scattering event cannot distinguish whether the scattering was caused by this distant polariton, or whether the distant polariton had already left and the scattering was instead caused by a newly formed polariton near the entrance [see Fig. S1(d)]. The resulting projection caused by the scattering hence acts simultaneously on the two polaritons leading to spatial entanglement [Fig. S1(d')].

As discussed in Appendix II, our model ignores such additional projections that can occur as the polariton leaves the first blockade radius of the medium. Since the rate of incoming photons determines both projection processes (the one occurring at the entrance into medium and the one occurring at the exit from the first blockade radius), we expect that ignoring the latter will not qualitatively affect our results.

II. DETERMINATION OF TRANSMISSION FUNCTION

In this Appendix, we present the details behind the derivation of the expressions for the average EIT transmission $\bar{\eta}_{\mathrm{EIT}}(l)$ for a medium of length l and the average effective blockade time $\bar{\tau}_{\mathrm{b}}$ given in Eqs. (5) and (6) of the main text.

To estimate these quantities, we rely on the intuition presented in Fig. 2(a,b) of the main text: That the temporal extent of the polariton wave function is determined near the beginning of the medium by its first R-R scattering event, whereas subsequent propagation within the first blockade radius is unaffected by any additional R-R scattering events. This suggests a serialized treatment of the R-R scattering and single-polariton EIT-filtering. Applying this approach, we take the temporal extent τ of a polariton to be defined by the first R-R event after its formation and assume its EIT transmission probability $\eta_{\mathrm{EIT}}(\tau, l)$ to be a function only of τ and the propagation length l in the medium. In doing so, we ignore the additional projections that can occur as the polariton leaves the first blockade radius of the medium, as discussed in Appendix I.

Averaging the EIT transmission probability $\eta_{\mathrm{EIT}}(\tau, l)$ over the CW/Poisson distribution for the timing of the first R-R scattering event τ amounts to

$$\bar{\eta}_{\mathrm{EIT}}(l) = \langle \eta_{\mathrm{EIT}}(\tau, l) \rangle_\tau = \int_0^\infty d\tau \mathcal{R}_{\mathrm{in}}(\mathcal{R}_{\mathrm{in}}\tau) e^{-\mathcal{R}_{\mathrm{in}}\tau} \eta_{\mathrm{EIT}}(\tau, l). \tag{S1}$$

From this average transmission probability, we estimate the average effective blockade time as

$$\bar{\tau}_{\mathrm{b}} = \tau_{\mathrm{b}} \int_0^{r_{\mathrm{b}}} \frac{dl}{r_{\mathrm{b}}} \bar{\eta}_{\mathrm{EIT}}(l). \tag{S2}$$

Approximating $\eta_{\mathrm{EIT}}(\tau, l)$ by the EIT transmission of a square pulse subjected to Gaussian filtering,

$$\eta_{\mathrm{EIT}}(\tau, l) = \int_0^\tau dt_1 \int_0^\tau dt_2 \frac{1}{\tau\sqrt{4\pi}\tau_{\mathrm{EIT}}(l)} \exp\left[-\frac{(t_1 - t_2)^2}{4\tau_{\mathrm{EIT}}^2(l)}\right] = \mathrm{Erf}\left[\frac{\tau}{2\tau_{\mathrm{EIT}}(l)}\right] - \frac{2\tau_{\mathrm{EIT}}(l)}{\sqrt{\pi}\tau}\left(1 - \exp\left[\frac{\tau^2}{4\tau_{\mathrm{EIT}}^2(l)}\right]\right), \tag{S3}$$

the integrals in Eqs. (S1,S2) can be evaluated, yielding the expressions given in Eqs. (5) and (6) of the main text.

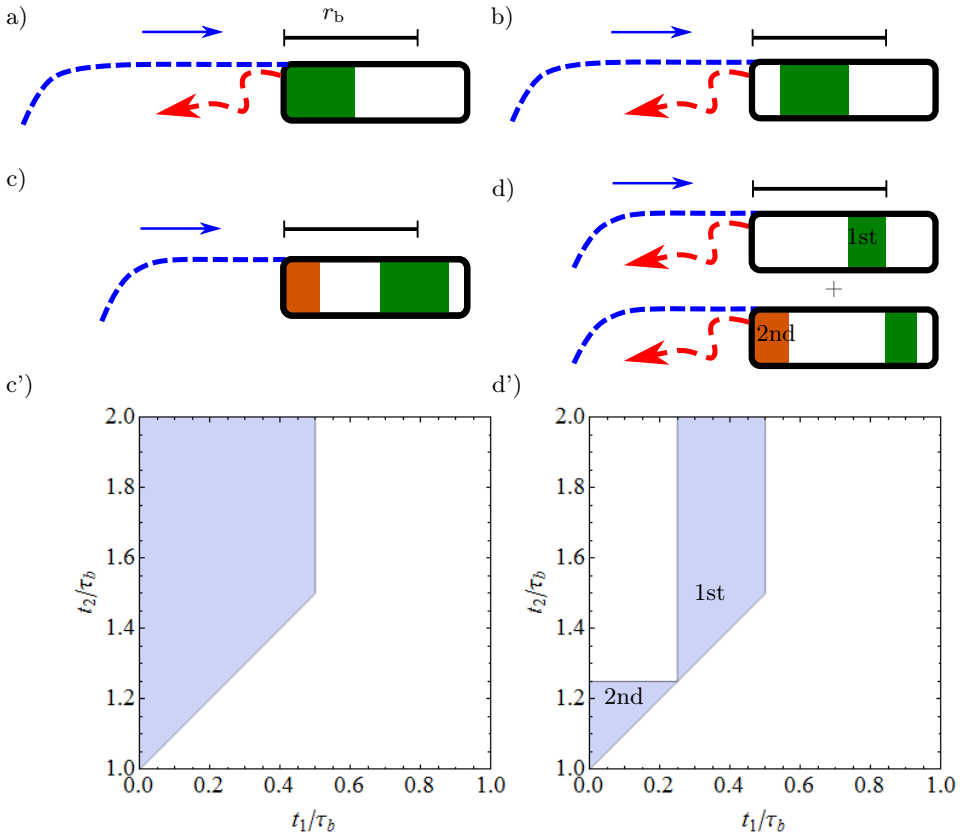

Figure S1. Formation of the polariton wave function by sequential projections of an incoming square pulse according to the hard-sphere model in the limit of perfect single-polariton EIT. (a) An incoming probe photon is scattered (red dashed arrow) near the beginning of the medium thereby projecting a polariton (green rectangle) in the medium. (b) The polariton propagates further into the medium, and, at a subsequent time, a second probe photon scatters, but since (in this instance) the polariton could not have left the first r_b of the medium, no additional projection of the polariton wave function ensues. (c) The polariton is now about to leave the first blockade radius of the medium, prompting us to consider possible formation times t_2 of the second polariton as described by the two-photon wave function in (c'), assuming the pulse to arrive at $t = 0$. The shaded region denotes the support of the wavefunction. (d) The first and second polaritons straddle the rear and front boundaries of the first blockade radius as a scattering event occurs; this causes a projection (c') $\rightarrow$ (d') on the two-body wave function producing a superposition state of the first and second polariton [as indicated in (d')] being the scatterer.

III. HARD-SPHERE CORRELATION FUNCTIONS

In this Appendix, we present the details behind the derivation of the first-order correlation function $G^{(1)}(\tau;\tau')$ presented in Eq. (7) of the main text, plot $G^{(1)}(\tau;\tau)$ for different parameters, and generalize the derivation to higher-order correlation functions. The derivations are carried out within the idealized hard-sphere dynamics for which single-polariton EIT effects are absent.

A. First-order correlation function

In this Section, we present the details behind the derivation of $G^{(1)}(\tau;\tau)$, Eq. (7) from the main text, and plot this function for different combinations of input rate and blockade time.

The same-time first-order correlation function $G^{(1)}(\tau;\tau)$ is given by the ensemble-averaged intensity profile $\langle\hat{I}(\tau)\rangle_{\hat{\rho}} = \langle\hat{\mathcal{E}}^\dagger(\tau)\hat{\mathcal{E}}(\tau)\rangle_{\hat{\rho}} = G^{(1)}(\tau;\tau)$, where the subscript signifies expectation value with respect to the density matrix $\hat{\rho}$ resulting from the hard-sphere interaction (ignoring EIT filtering). For square-pulse Poisson input (of rate $\mathcal{R}_{\rm in}$), this function can be derived inductively by propagating the initial condition that the medium is empty when the input pulse arrives at the medium at time τ_s (and using the fact that different segments of the input pulse are uncorrelated). Let us first consider the probability density $P_1(t_1 - \tau_s)$ of the first Rydberg excitation occurring at a time $t_1 \geq \tau_s$; this is simply the product of the probability that no photons arrived during the interval $[\tau_s; t_1]$, i.e. $\exp[-\mathcal{R}_{\rm in}(t_1 - \tau_s)]$ for

the Poisson distribution, and the arrival rate of photons $\mathcal{R}_{\rm in}$, so that we have

$$P_1(\tau) = \theta(\tau)\mathcal{R}_{\rm in}\exp[-r\tau], \tag{S4}$$

where $\theta(\tau)$ is the Heaviside step function with the convention $\theta(0) = 1$. Next, let us construct the probability density $P_2(t_2 - \tau_{\rm s})$ that the second Rydberg excitation occurs at time t_2. Note that, per the hard-sphere ansatz, this probability density can be non-zero only for $t_2 \geq \tau_{\rm s} + \tau_{\rm b}$. The *conditional* probability density of the second Rydberg excitation occurring at t_2 conditioned on the first Rydberg excitation arriving at t_1 is just $P_1(t_2 - t_1 - \tau_{\rm b})$, where P_1 is given in Eq. (S4); i.e. the first Rydberg excitation (at t_1) imposes an initial condition of an empty medium at $t_1 + \tau_{\rm b}$ equivalent to the one at $\tau_{\rm s}$. The unconditional probability density $P_2(t_2 - \tau_{\rm s})$ for the arrival of the second Rydberg at t_2 is then found by integrating the conditional density $P_1(t_2 - t_1 - \tau_{\rm b})$ over $t_1 \in [\tau_{\rm s}, t_2 - \tau_{\rm b}]$ weighted by the probability density $P_1(t_1 - \tau_{\rm s})$ we found above for t_1,

$$\begin{aligned} P_2(t_2 - \tau_{\rm s}) &= \theta(t_2 - \tau_{\rm s} - \tau_{\rm b})\int_{\tau_{\rm s}}^{t-\tau_{\rm b}} dt_1 P_1(t_1 - \tau_{\rm s}) \times P_1(t_2 - t_1 - \tau_{\rm b}) \\ &= \theta(t_2 - \tau_{\rm s} - \tau_{\rm b})\mathcal{R}_{\rm in}\exp[-\mathcal{R}_{\rm in}(t_2 - \tau_{\rm s} - \tau_{\rm b})] \times [\mathcal{R}_{\rm in}(t_2 - \tau_{\rm s} - \tau_{\rm b})]. \end{aligned} \tag{S5}$$

By iterating this argument, we find the probability density for the arrival of the R'th Rydberg excitation at time t_R to be given by (defining $t_0 \equiv \tau_{\rm s} - \tau_{\rm b}$ for convenience)

$$P_R(t_R - \tau_{\rm s}) = \theta(t_R - \tau_{\rm s} - (R-1)\tau_{\rm b})\mathcal{R}_{\rm in}e^{-\mathcal{R}_{\rm in}(t_R - \tau_{\rm s} - (R-1)\tau_{\rm b})}\frac{[\mathcal{R}_{\rm in}(t_R - \tau_{\rm s} - (R-1)\tau_{\rm b})]^{R-1}}{(R-1)!}. \tag{S6}$$

$P_R(t_R - \tau_{\rm s})$ in Eq. (S6) is the probability density of the creation of a polariton at time t_R conditioned on $R-1$ polaritons having been created in the preceding time interval $[\tau_{\rm s}, t_R - \tau_{\rm b}]$. This allows us to construct $G^{(1)}(\tau;\tau)$ simply by observing that its value at a time $\tau = t - \tau_{\rm s}$ after the onset of the pulse only can have contributions from the first $\lceil (t-\tau_{\rm s})/\tau_{\rm b}\rceil$ polaritons created since $\tau_{\rm s}$ per the hard-sphere ansatz; summing these contributions, Eq. (S6), we find ($t \geq \tau_{\rm s}$)

$$G^{(1)}(t - \tau_{\rm s}; t - \tau_{\rm s}) = \sum_{j=1}^{\lceil (t-\tau_{\rm s})/\tau_{\rm b}\rceil} P_j(t - \tau_{\rm s}) = \sum_{j'=0}^{\lfloor (t-\tau_{\rm s})/\tau_{\rm b}\rfloor} \mathcal{R}_{\rm in}e^{-\mathcal{R}_{\rm in}(t - \tau_{\rm s} - j'\tau_{\rm b})}\frac{[\mathcal{R}_{\rm in}(t - \tau_{\rm s} - j'\tau_{\rm b})]^{j'}}{j'!}, \tag{S7}$$

also given in Eq. (7) of the main text (setting $\tau_{\rm s} = 0$ for simplicity). We plot Eq. (S7) in Fig. S2 for different combinations of the input rate $\mathcal{R}_{\rm in}$ and the blockade time in units of pulse duration $\tau_{\rm b}/\tau_{\rm p}$. The width of the peaks are seen to increase with peak number while their heights decrease. This is a symptom of the decay of the initial condition of a vacant medium at $\tau_{\rm s}$ when the pulse arrives, corresponding to the decay of photon-photon correlations in the output signal.

The off-diagonal elements $G^{(1)}(t - \tau_{\rm s}; t' - \tau_{\rm s})$ can be expressed conveniently in terms of the diagonal elements (S7)

$$G^{(1)}(t - \tau_{\rm s}; t' - \tau_{\rm s}) = G^{(1)}(t_< - \tau_{\rm s}; t_< - \tau_{\rm s})e^{-2\mathcal{R}_{\rm in}\min\{|t-t'|, \tau_{\rm b}\}} \times \begin{cases} 1, & \text{if } |t-t'| \leq \tau_{\rm b} \\ \mathcal{R}_{\rm in}^{-1}G^{(1)}(|t-t'| - \tau_{\rm b}; |t-t'| - \tau_{\rm b}), & \text{if } |t-t'| > \tau_{\rm b} \end{cases}, \tag{S8}$$

where $t_< \equiv \min\{t, t'\}$. Eq. (S8) is derived in the main text for the special case $|t - t'| \leq \tau_{\rm b}$, see Eq. (8). In the case $|t - t'| > \tau_{\rm b}$ we must account for the fact that not all event histories for the intermediate time interval $[\min\{t,t'\} + \tau_{\rm b}; \max\{t,t'\}]$ are compatible with the medium being vacant at $\max\{t,t'\}$; hence we multiply by the probability that this is the case conditioned on the medium being vacant at $\min\{t,t'\} + \tau_{\rm b}$, i.e., $\mathcal{R}_{\rm in}^{-1}G^{(1)}(|t-t'| - \tau_{\rm b}; |t-t'| - \tau_{\rm b})$.

B. Higher-order correlation functions

In this Section, we extend the arguments of the previous section to derive higher-order correlation functions, a possibility mentioned in conjunction with Eq. (7) of the main text.

The second-order correlation function,

$$G^{(2)}(\tau_1, \tau_2; \tau_2, \tau_1) = \langle :: \hat{I}(\tau_1)\hat{I}(\tau_2) :: \rangle_{\hat{\rho}} = \langle \hat{\mathcal{E}}^\dagger(\tau_1)\hat{\mathcal{E}}^\dagger(\tau_2)\hat{\mathcal{E}}(\tau_2)\hat{\mathcal{E}}(\tau_1)\rangle_{\hat{\rho}}, \tag{S9}$$

can be constructed from the diagonal elements $G^{(1)}(\tau;\tau)$ derived in Eq. (S7) by pursuing a similar logic: As the product between the probability density of creating a polariton at time $\tau_{\rm s} + \min\{\tau_1, \tau_2\}$ conditioned on a vacant

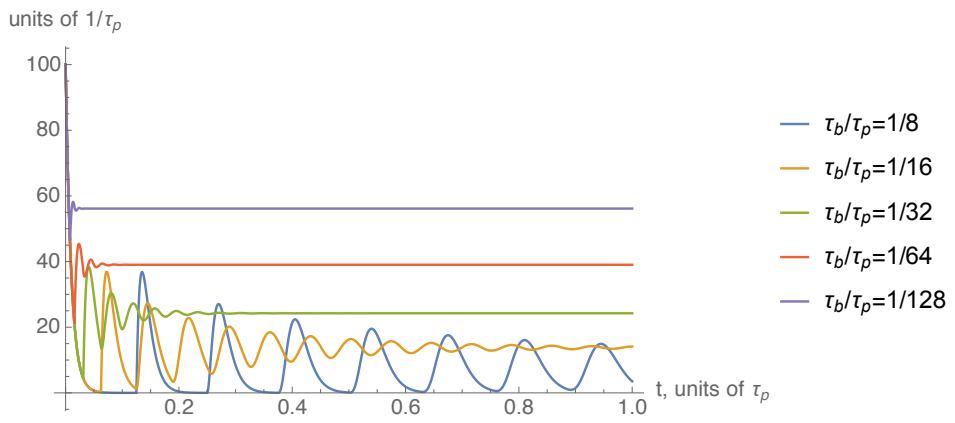

Figure S2. Ensemble-averaged output intensity $\langle \hat{I}(t)\rangle_{\hat{\rho}} \equiv G^{(1)}(t;t)$ according to the hard-sphere ansatz (ignoring EIT filtering). Poisson-distributed input with fixed mean number of photons $\mathcal{R}_{\rm in}\tau_{\rm p} = 100$ for different ratios of blockade time to pulse duration, $\tau_{\rm b}/\tau_{\rm p}$.

medium at $\tau_{\rm s}$ and the probability density of creating a polariton at time $\tau_{\rm s} + \max\{\tau_1, \tau_2\}$ conditioned on a polariton having been created at $\tau_{\rm s} + \min\{\tau_1, \tau_2\}$. Importantly, the latter is independent of the event history of the time interval $[\tau_{\rm s}; \tau_{\rm s} + \min\{\tau_1, \tau_2\} + \tau_{\rm b}]$. This is because the counting statistics of different time intervals of the CW input are uncorrelated and conditioning on having a Rydberg excitation created at $\tau_{\rm s}+\min\{\tau_1, \tau_2\}$ sets a boundary condition at $t' = \tau_{\rm s} + \min\{\tau_1, \tau_2\} + \tau_{\rm b}$ equivalent to the initial condition at $\tau_{\rm s}$ of a vacant Rydberg medium. This argument leads to the expression:

$$G^{(2)}(\tau_1, \tau_2; \tau_2, \tau_1) = \Theta(|\tau_2 - \tau_1| - \tau_{\rm b}) G^{(1)}(\min\{\tau_1, \tau_2\}; \min\{\tau_1, \tau_2\}) G^{(1)}(|\tau_2 - \tau_1| - \tau_{\rm b}; |\tau_2 - \tau_1| - \tau_{\rm b}). \tag{S10}$$

This argument can be iterated to express the "diagonal" elements ($\tau_i = \tau_i'$) of the correlation function

$$G^{(N)}(\tau_1, \ldots, \tau_N; \tau_N', \ldots, \tau_1') \equiv \langle :: \prod_{i=1}^{N} \hat{\mathcal{E}}^\dagger(\tau_i) \hat{\mathcal{E}}(\tau_i') :: \rangle_{\hat{\rho}} \tag{S11}$$

in terms of those of $G^{(1)}$ found in Eq. (S7). Assuming a time-ordered set $\{\tau_1, \ldots, \tau_N\}$, Eq. (S10) generalizes to (where $\tau_0 \equiv -\tau_{\rm b}$ for convenience)

$$G^{(N)}(\tau_1, \ldots, \tau_N; \tau_N, \ldots, \tau_1) = \prod_{i=1}^{N} \theta(\tau_i - \tau_{i-1} - \tau_{\rm b}) G^{(1)}(\tau_i - \tau_{i-1} - \tau_{\rm b}; \tau_i - \tau_{i-1} - \tau_{\rm b}). \tag{S12}$$

IV. COMPARISON TO NUMERICAL SIMULATIONS OF 3-LEVEL MODEL FOR 2-PHOTON INPUT

To check the serialization approximation for EIT filtering used when analyzing the scheme for generating single-photon trains, we compare the results of this approximation against numerical simulations of the full set of equations of motion. The serialization approximation amounts to passing the state generated by the idealized R-R interaction [Fig. S1] through a linear EIT filter.

For the comparison, we consider square-pulse two-photon Fock-state input with (which is reasonably feasible numerically). To establish the prediction from our model, consider (for generality) an arbitrary temporal pulse shape $h(t)$ which is non-zero only in the time interval $[0; \tau_{\rm end} \geq \tau_{\rm b}]$ (normalized as $\int h^2(t)dt = 1$). According to the hard-sphere ansatz (ignoring single-polariton EIT decay) the density matrix when the entire pulse has entered the medium is

$$\hat{\rho}(t) = \overbrace{2\int_0^{\tau_{\rm end}} d\tau_1 \int_{\max\{\tau_1-\tau_{\rm b},0\}}^{\tau_1} dt_1 h^2(\tau_1)h^2(t_1)|\tilde{\psi}_{\tau_1}(t)\rangle\langle\tilde{\psi}_{\tau_1}(t)|}^{\text{one scattering event}} + \overbrace{2\int_0^{\tau_{\rm end}-\tau_{\rm b}} dt_1 \int_{t_1+\tau_{\rm b}}^{\tau_{\rm end}} dt_2 h^2(t_1)h^2(t_2)|\tilde{\psi}_{\emptyset}(t)\rangle\langle\tilde{\psi}_{\emptyset}(t)|}^{\text{no scattering event, }\emptyset}, \tag{S13}$$

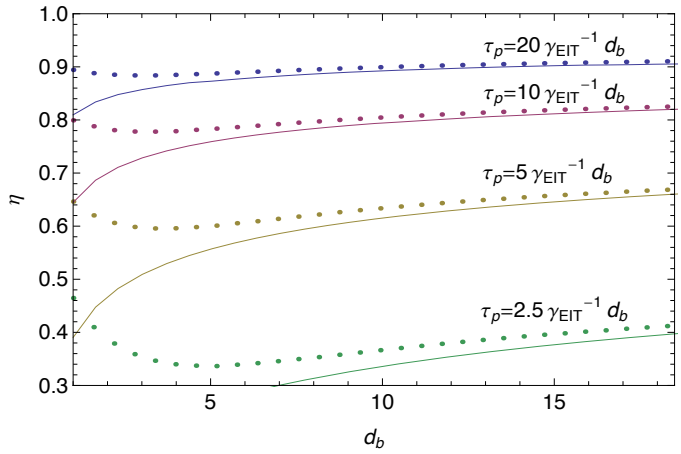

Figure S3. Transmission through a dissipative Rydberg-EIT medium. Comparison between full numerical simulation and hard-sphere ansatz with post-EIT-filtering for the propagation of a two-photon square pulse through a Rydberg medium of length $L = r_\mathrm{b}$.

where the normalized wave functions are

$$|\tilde{\psi}_{\tau_1}(t)\rangle = \frac{-\sqrt{v_\mathrm{g}}}{\sqrt{\int_{\max\{\tau_1-\tau_\mathrm{b},0\}}^{\tau_1} dt_1' h^2(t_1')}} \int_{\max\{\tau_1-\tau_\mathrm{b},0\}}^{\tau_1} dt_1 h(t_1) \hat{S}^\dagger[v_\mathrm{g}(t-t_1)]|0\rangle, \tag{S14}$$

$$|\tilde{\psi}_{\emptyset}(t)\rangle = \frac{v_\mathrm{g}}{\sqrt{\int_0^{\tau_\mathrm{end}-\tau_\mathrm{b}} dt_1' \int_{t_1'+\tau_\mathrm{b}}^{\tau_\mathrm{end}} dt_2' h^2(t_1')h^2(t_2')}} \int_0^{\tau_\mathrm{end}-\tau_\mathrm{b}} dt_1 \int_{t_1+\tau_\mathrm{b}}^{\tau_\mathrm{end}} dt_2 h(t_1)h(t_2) \hat{S}^\dagger[v_\mathrm{g}(t-t_1)]\hat{S}^\dagger[v_\mathrm{g}(t-t_2)]|0\rangle. \tag{S15}$$

For our special case of a square pulse we have $h(t) = \tau_\mathrm{end}^{-1/2}$, in which case the above integrals can be straightforwardly calculated. We subject $\hat{\rho}$ given in Eq. (S13) to linear EIT filtering corresponding to the full length L of the Rydberg medium (taking $L = r_\mathrm{b}$). We focus on the transmission of the two-photon component, i.e., the probability that neither R-R scattering nor EIT decay occurs. This amounts to filtering the second term in Eq. (S13), i.e., for square-pulse input, filtering the (unnormalized) wavefunction of the state $(1-\tau_\mathrm{b}/\tau_\mathrm{end})|\tilde{\psi}_\emptyset(t)\rangle$, where $|\tilde{\psi}_\emptyset(t)\rangle$ is given in Eq. (S15). The square norm of the filtered wavefunction is the desired transmission probability. For simplicity, we approximated the effect of a linear EIT medium by a Gaussian filter, yielding the curves presented in Fig. S3. This serialized approximation yields a pessimistic estimate, since the sharp temporal features removed by the filter are in general created somewhere in the interior of the medium thus reducing the effective optical depth of the EIT-filtering effect.

The above theoretical prediction for square-pulse 2-photon Fock-state input is compared to time-dependent numerical simulations of the pulse transmission through the medium using a three-level model for the atoms. The numerical methods are detailed in the supplementary material of Refs. [S1, S2]. The comparison is shown in Fig. S3, where we plot the transmission of the two-photon component, showing good agreement for $d_\mathrm{b} \gtrsim 10$.

V. GENERATION OF TRAINS OF SINGLE PHOTONS FROM CW INPUT

In this Appendix, we present the details behind the derivation of the requirements that the input rate $\mathcal{R}_\mathrm{in}$ has to satisfy in order to produce a regular train of single photons from CW input. Combining these requirements yield the scaling result presented as Eq. (9) in the main text.

Since $G^{(N)}$ is simply related to $G^{(1)}$ by Eq. (S12), we will consider the signatures of regularity in $G^{(1)}$. Considering the individual (unit-area) polariton peak profiles $P_j(t-\tau_\mathrm{s})$ in Eq. (S7), the j'th peak is seen to be located at $t_j = \tau_\mathrm{s} + j(\tau_\mathrm{b} + 1/\mathcal{R}_\mathrm{in})$ and hence the peak-to-peak separation is $\Delta t = \tau_\mathrm{b} + 1/\mathcal{R}_\mathrm{in}$. In the high-intensity limit, the peaks are well-separated, and we can approximate Eq. (S7) by

$$\langle \hat{I}(\tau \sim t_p - \tau_\mathrm{s})\rangle_{\hat{\rho}} \equiv G^{(1)}(\tau;\tau) \approx P_p(\tau), \tag{S16}$$

where $\tau \sim t_p - \tau_\mathrm{s}$ means that τ is in the neighborhood of the p'th peak at $t_p - \tau_\mathrm{p}$ (or, more precisely, that p minimizes $|\tau - t_p + \tau_\mathrm{s}|$).

A. Localization condition

To derive a condition for well-separated peaks, we consider the corrections to Eq. (S16), which are simply the tails of the other P_j in Eq. (S7):

$$\langle \hat{I}(\tau \sim t_p - \tau_\mathrm{s})\rangle_{\hat{\rho}} = P_p(\tau) + \sum_{j=1, j\neq p}^{\lceil \tau/\tau_\mathrm{b}\rceil} P_j(\tau). \tag{S17}$$

As we shall see shortly, the width of $P_p(t)$ is sublinear in p ($\sim \sqrt{p}$) and hence grows slower than $t_p - \tau_\mathrm{s} \propto p$. For this reason, it is sufficient to ensure that each peak $P_p(t)$ is well-separated from its nearest neighbors. Thus, to have a train of N well-separated photons, we must ensure that the width $(\delta t)_N$ of the last peak P_N is much less than the peak separation, $(\delta t)_N \ll \Delta t \approx \tau_\mathrm{b}$ (in the high-intensity limit, $\mathcal{R}_\mathrm{in} \gg 1/\tau_\mathrm{b}$). Since the p'th peak width (HWHM) can be approximated for $p \gg 1$ from Eq. (S6) as

$$(\delta t)_p \approx \frac{\sqrt{\ln(4)p}}{\mathcal{R}_\mathrm{in}}, \tag{S18}$$

this leads to the lower bound for $\mathcal{R}_\mathrm{in}$ presented in the main text (omitting the factor $\sqrt{\ln(4)} \sim 1$ for simplicity).

B. EIT transmittivity condition

We now present the details behind the input rate requirement imposed by the finite EIT window. Using Eq. (8) of the main text in the limit of well-separated peaks for which Eq. (S16) is applicable, we may filter the peaks individually (here assuming $\tau_\mathrm{EIT} \ll \tau_\mathrm{b}$ and using the Gaussian EIT approximation),

$$\tilde{P}_p(\tau) \approx \int_{-\infty}^{\infty} dt_1 \int_{-\infty}^{\infty} dt_2 P_p(\min\{t_1, t_2\}) e^{-2\mathcal{R}_\mathrm{in}|t_1 - t_2|} \frac{1}{2\pi\tau_\mathrm{EIT}^2} e^{-\frac{(t_1-\tau)^2}{2\tau_\mathrm{EIT}^2}} e^{-\frac{(t_2-\tau)^2}{2\tau_\mathrm{EIT}^2}}. \tag{S19}$$

Using Eq. (S19) we estimate the single-polariton EIT transmission $\bar{\eta}_\mathrm{EIT}$ as the integral over an individual filtered intensity peak $\tilde{P}_p(\tau)$ [S3],

$$\bar{\eta}_\mathrm{EIT} \equiv \int_{-\infty}^{\infty} d\tau \tilde{P}_p(\tau) = \exp\left([2\tau_\mathrm{EIT}\mathcal{R}_\mathrm{in}]^2\right) \mathrm{erfc}\left(2\tau_\mathrm{EIT}\mathcal{R}_\mathrm{in}\right), \tag{S20}$$

which is independent of the peak number p. Expanding this in the limit $\tau_\mathrm{EIT} \ll 1/\mathcal{R}_\mathrm{in}$ we find that

$$\bar{\eta}_\mathrm{EIT} \approx 1 - \frac{4\mathcal{R}_\mathrm{in}\tau_\mathrm{EIT}}{\sqrt{\pi}} + \mathcal{O}[(\mathcal{R}_\mathrm{in}\tau_\mathrm{EIT})^2]. \tag{S21}$$

Tolerating an EIT loss fraction of at most $\epsilon = 1 - \bar{\eta}_\mathrm{EIT}$, we are faced with an upper bound for $\mathcal{R}_\mathrm{in}$,

$$\mathcal{R}_\mathrm{in} \lesssim \frac{\sqrt{\pi}}{4}\frac{\epsilon}{\tau_\mathrm{EIT}}, \tag{S22}$$

as presented in the main text (again omitting factors of order unity for simplicity).

[S1] T. Peyronel, O. Firstenberg, Q.-Y. Liang, S. Hofferberth, A. V. Gorshkov, T. Pohl, M. D. Lukin, and V. Vuletic, Nature **488**, 57 (2012).

[S2] M. F. Maghrebi, M. J. Gullans, P. Bienias, S. Choi, I. Martin, O. Firstenberg, M. D. Lukin, H. P. Büchler, and A. V. Gorshkov, Phys. Rev. Lett. **115**, 123601 (2015).

[S3] The EIT loss determined here by post-filtering is found to be a factor of 2 worse than $\bar{\eta}_\mathrm{EIT}(r_\mathrm{b})$ as given by Eq. (S1) (comparing leading order terms in $\mathcal{R}_\mathrm{in}\tau_\mathrm{EIT}$). We ascribe this to the additional projections that can occur when a polariton leaves the first r_b of the medium [see Appendix I and Fig. S1(d)].